Research Square

Preprints are preliminary reports that have not undergone peer review.
They should not be considered conclusive, used to inform clinical practice,
or referenced by the media as validated information.

Satellite-derived methane emissions reveal persistent gaps in global oil and gas mitigation performance

Mark Omara

momara@edf.org

Environmental Defense Fund https://orcid.org/0000-0002-8933-1927

James P. Williams

https://orcid.org/0000-0002-1746-0420

Anthony Himmelberger

MethaneSAT, LLC

Kaiya Weatherby

Environmental Defense Fund

Ben Lyke

Environmental Defense Fund

Jack Warren

Environmental Defense Fund

Katlyn MacKay

Environmental Defense Fund

Luis Guanter

Environmental Defense Fund

Joshua Benmergui

Environmental Defense Fund

Marvin Knapp

Harvard John A. Paulson School of Engineering and Applied Sciences, Harvard University

Christopher Miller

Harvard John A. Paulson School of Engineering and Applied Sciences, Harvard University

Sebastien Roche

Environmental Defense Fund https://orcid.org/0000-0003-2474-4744

Jonathan Franklin

Harvard University

Steven Hamburg

Environmental Defense Fund

Steven Wofsy

Harvard University

Ritesh Gautam

Environmental Defense Fund

Article

Keywords:

Posted Date: May 14th, 2026

DOI: https://doi.org/10.21203/rs.3.rs-9688202/v1

License: This work is licensed under a Creative Commons Attribution 4.0 International License.
Read Full License

Additional Declarations: There is **NO** Competing Interest.

Satellite-derived methane emissions reveal persistent gaps in global oil and gas mitigation performance

Mark Omara[1,2], James P. Williams[1,2], Anthony Himmelberger[2], Kaiya Weatherby[1,2], Ben Lyke[1,2], Jack Warren[1,2], Katlyn MacKay[1,2], Luis Guanter[1,3], Joshua Benmergui[1,2,4], Marvin Knapp[1,2,4], Christopher C. Miller[1,2,4], Sèbastien Roche[1,2,4], Jonathan Franklin[4], Steven P. Hamburg[1,2], Steven C. Wofsy[4], Ritesh Gautam[1,2]

[1] Environmental Defense Fund, New York, NY 10010, USA
[2] MethaneSAT, LLC, Austin, TX 78701, USA
[3] Research Institute of Water and Environmental Engineering (IIAMA), Universitat Politecnica de Valencia, Valencia, Spain
[4] Harvard John A. Paulson School of Engineering and Applied Sciences, Harvard University, Cambridge, MA 02138, USA

Correspondence to: Mark Omara (momara@edf.org)

Abstract

Mitigating methane emissions from global oil and gas operations remains a critical climate priority, given methane's high radiative efficiency and short atmospheric lifetime. Using MethaneSAT satellite observations (March 2024–June 2025), we quantify emissions across 34 regions representing ~50% of global onshore oil and gas production. Regional emissions vary by nearly two orders of magnitude (~5 to >400 t h^{-1}), and the largest producing regions are also among the largest emitters. MethaneSAT estimates exceed reported "bottom-up" inventories by ~60%, with large regional differences, especially between oil-dominated and gas or mixed-production regions. Several regions show anomalously high methane intensity relative to production, identifying priority mitigation targets across North America, South America, Central Asia, and the Middle East. Across all regions, mean methane intensity is 2.9% of marketed gas (95% CI: 2.4–3.3%) and 0.19 kg GJ^{-1} (0.16–0.22), ~10× higher than the Oil and Gas Decarbonization Charter target (0.2%). These results reveal major gaps in current methane management and underscore the scale of reductions required for alignment with commitments under the OGDC and the Global Methane Pledge.

Introduction

Methane emissions from global oil and gas operations have come under sustained scrutiny in recent years due to methane's high radiative efficiency and short atmospheric lifetime, which together make it one of the most effective levers for near-term climate mitigation[1,2,3]. Recent research demonstrates that a large fraction of oil and gas methane emissions can be mitigated using readily available and cost-effective technologies[4,5,6]. In alignment with the objective of limiting global temperature rise to 1.5 ºC above pre-industrial levels under the Paris Agreement,[7] rapid reductions in methane emissions have become an explicit policy priority across major oil and gas producing jurisdictions.

This urgency has catalyzed coordinated action by governments and the oil and gas industry. Focused international initiatives—including the Oil and Gas Decarbonization Charter (OGDC)[8] and the Global Methane Pledge (GMP)[9] have established quantitative targets and sector-specific commitments to reduce methane emissions this decade. Central to the credibility and effectiveness of these pledges and commitments is the ability to assess, validate, and independently verify reported emissions against stated mitigation targets. Robust measurement-based methane monitoring frameworks are thus indispensable for tracking progress, identifying mitigation opportunities, and ensuring accountability.

Independent assessment of oil and gas methane emissions requires comprehensive measurements across multiple spatial scales, from equipment and facility levels to basin and regional aggregates. While bottom-up inventories remain the basis of national reporting, they are often subject to uncertainties related to emission factors, activity data, and incomplete representation of dispersed area emissions and super-emitting events[10-14]. In recent years, satellite remote sensing has emerged as a transformative capability for global methane monitoring. Space-based observations enable systematic detection of high-emitting point sources,[15-18] dispersed area source emissions, and quantification of total regional methane fluxes[19-21], providing an independent constraint on inventory estimates and facilitating cross-regional comparisons.

In this study, we present a global-scale assessment of regional oil and gas methane emissions derived from observations by MethaneSAT (www.methanesat.org), representing 50 percent of global onshore oil and gas production. MethaneSAT collected targeted observations over major oil and gas production regions between March 2024, following launch, and June 2025, when operations ceased after loss of communication with the satellite. The instrument combined wide-area coverage (approximately 220 km × 220 km at nadir) with high native spatial resolution (110 m × 400 m at nadir) and precision (2.5–5.5 ppb at 2 km × 2 km aggregation)[22], enabling

high-spatial resolution characterization of total methane emissions across diverse geological, operational, and regulatory contexts worldwide. The principal MethaneSAT data products include: (i) gridded methane emission fluxes at 4 km × 4 km resolution for basin- and regional-scale area sources[20] and (ii) quantification of discrete high-emitting point sources[18]. Together, these products provide an internally consistent (dispersed area emissions and discrete high-emitting point source emissions) dataset for evaluating both aggregate regional methane emissions, their spatial distribution, and further enable the assessment of oil and gas methane intensity metrics that are policy-relevant for evaluating methane mitigation targets.

We analyze oil and gas methane emission fluxes across 34 production regions globally to address three primary objectives. First, we characterize regional-scale emission patterns and assess the magnitude and variability of emissions across regions. Second, we compare satellite-derived emission estimates with commonly referenced “bottom-up” inventories to quantify discrepancies and examine potential drivers. Third, we evaluate methane intensities across regions and assess their implications for meeting stated abatement pledges and commitments. By integrating high-resolution satellite-derived methane emissions across major global oil and gas production regions, this work provides an independent, measurement-based characterization of regional variability in oil and gas methane emissions viz-a-viz inventory reporting and evaluating progress toward oil and gas methane mitigation goals.

Results and discussion

Wide variability in regional total oil and gas methane emissions.

MethaneSAT’s ability to resolve both diffuse, lower-emission area sources and discrete, high-emitting point sources enables an integrated high-spatial-resolution characterization of regional total methane fluxes. Using these capabilities and based on observations between May 2024 and June 2025, we analyze methane emissions from 34 major oil and gas production regions that collectively account for approximately 50 percent of global onshore marketed oil and gas output[23] (Fig. 1), providing a representative cross-section of contemporary oil and gas extraction practices and methane emitting regions.

The regions included in this assessment span more than two orders of magnitude in oil and gas production volume—from ~50 petajoules per year (PJ yr^{-1}; 1 barrels of oil equivalent ~ 5.7×10^{-6} PJ) in smaller regions to over 23,000 PJ yr^{-1} in the most intensively developed systems—and range in area from ~16,000 to 190,000 km^2. Collectively, the 34 aggregated domains cover 2,538,000 km^2—about the same area as 12 Permian Basin (U.S.) regions.

These regions exhibit marked contrasts in oil and gas production characteristics. Predominantly oil-producing regions (n = 10) are defined by gas contributing <20% of total marketed energy output, whereas gas-dominated regions (n = 7) exceed 80%. Mixed-production regions (n = 17) fall between these bounds (Fig. 1). This breadth in geological context, infrastructure maturity, and operational profile constitutes an ideal framework for assessing how methane emissions vary by region and scale with oil and gas production and other operational characteristics.

Figure 1 (panels **a, c, and e**) presents examples of MethaneSAT's regional methane emission quantification, demonstrating its characteristic fine spatial resolution (4 km × 4 km) across basin-scale. For each region, we disaggregate the total methane emissions to sectoral methane emissions (oil and gas methane and non-oil and gas emissions) by incorporating prior information from peer-reviewed assessments of methane emission sources at both regional and gridded scales (Methods).

Across all 34 regions, we estimate total oil and gas methane emissions equivalent to 24 Tg per year (95% confidence interval: 20—28 Tg per year). At the regional level, oil and gas methane emissions vary by more than two orders of magnitude, from approximately 5 t h^{-1} to over 400 t h^{-1} (Fig. 2). The regions with the highest oil and gas methane emissions—such as the Permian Basin (U.S.) and the Widyan region (Iran and Iraq)—are also among the world's largest oil and gas producers (Fig. 2; Fig. 3a). At these regional scales, we observe a positive correlation between methane emissions and total marketed oil and gas production (R = 0.5, $p < 0.001$; Fig. 3a). This relationship suggests that extensive oil and gas infrastructure networks and high throughput increase both the frequency and magnitude of methane emission events. However, substantial variability exists among regions with similar oil and gas production levels (as shown by the degree of scatter in Fig. 3a), indicating that other factors beyond production volume also influence methane emissions at these scales.

We also identify evidence of exceptionally large facility-level methane venting events, generally exceeding 1 tonne per hour per facility, in several of the highest-emitting regions (Supplementary Note 4, Supplementary Fig. 5). Notably, these include the Permian Basin in the U.S., the Maturín region of Venezuela, the South Caspian region of Turkmenistan, and in the Widyan/Zagros Foldbelt regions of Iran and Iraq. Detailed analyses of these high-emission point sources based on MethaneSAT data analyzed herein are provided in Guanter et al.[18] When combined with the evidence of large gas flaring volumes in these same regions (Fig. 2, based on VIIRS satellite observations[25]), our findings suggest that substantial volumes of methane emissions in these regions are avoidable, underscoring a significant and actionable opportunity for mitigation.

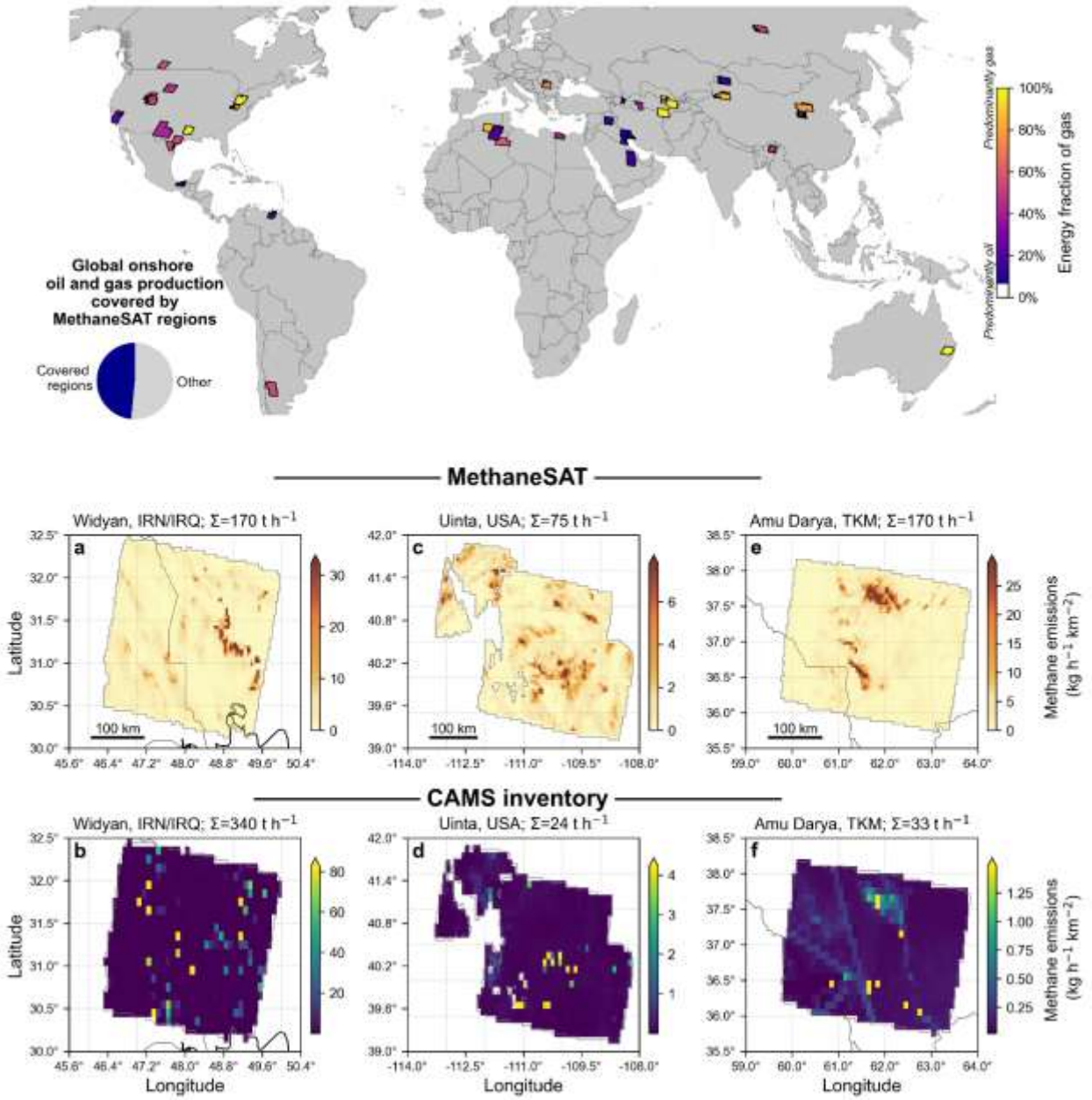


Figure 1. Global map showing the 34 regions observed by MethaneSAT between May 2024 and June 2025. Regions are color-coded by the proportion of total marketed energy derived from gas production (energy fraction of gas): warmer colors indicate predominantly gas-producing regions, while cooler colors represent predominantly oil-producing regions. The lower panels provide examples of regional total methane flux quantification from MethaneSAT (middle panel) and the CAMS[24] inventory (bottom panel) for three representative regions: a predominantly oil-producing region (Widyan, Iran/Iraq; panels **a** and **b**), a mixed oil and gas region (Uinta, USA; panels **c** and **d**), and a predominantly gas-producing region (Amu Darya, Turkmenistan; panels **e** and **f**). MethaneSAT flux estimates are gridded at 4 km × 4 km resolution whereas CAMS fluxes are gridded at approximately 10 km × 10 km resolution. We use the CAMS inventory here to facilitate comparison of total methane emissions with the MethaneSAT results. IRN—Iran; IRQ—Iraq; TKM—Turkmenistan; USA—United States of America.

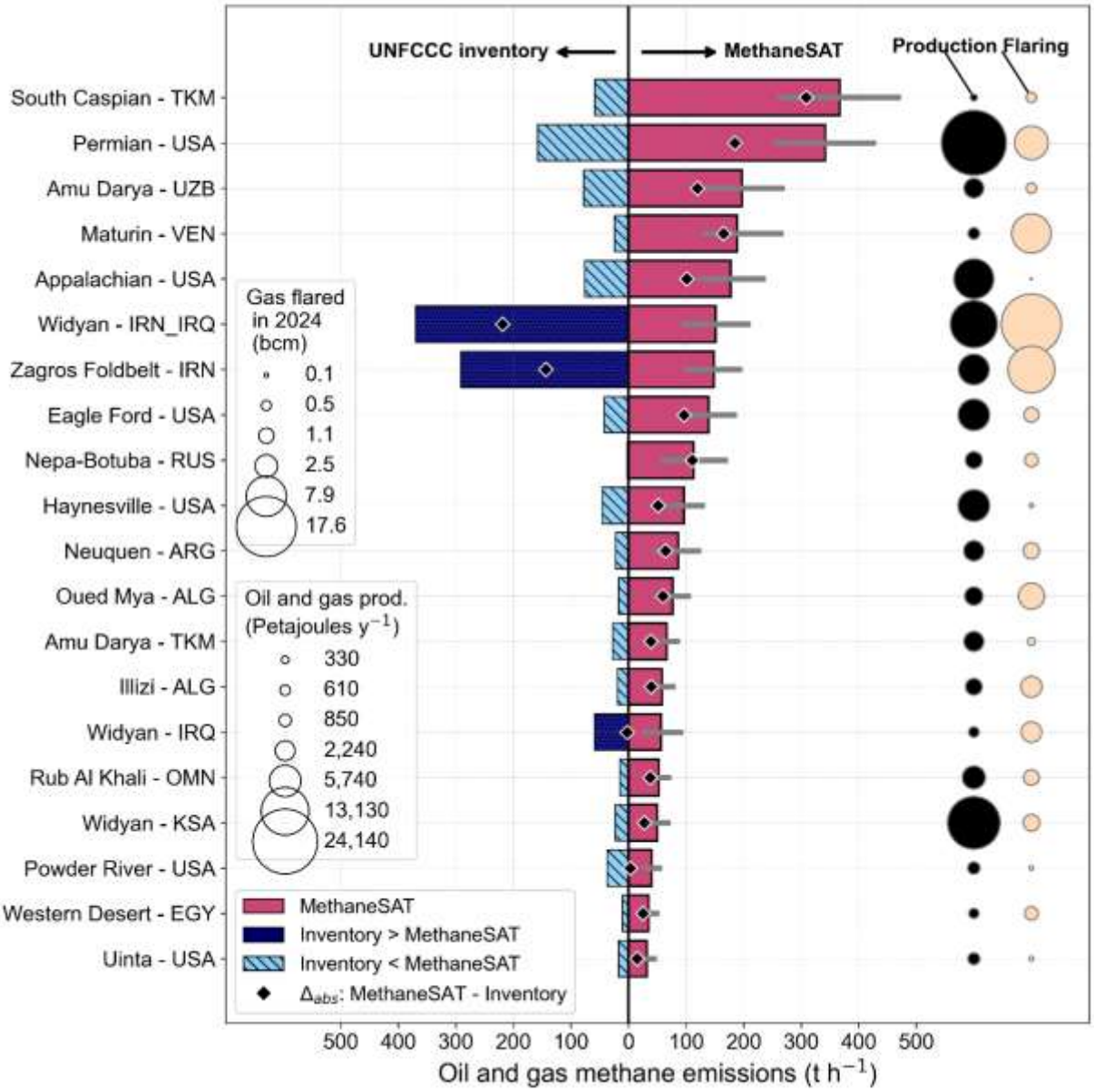


Figure 2. Comparison of regional oil and gas methane emissions for the 20 highest-emitting regions (out of 34), each with estimated emissions exceeding 30 tonnes per hour. MethaneSAT estimates are shown as purple bars, with error bars indicating the 95% confidence interval of the mean. For all regions, inventory values are derived from the gridded country-reported inventories to the UNFCCC, as reported in the GFEI inventory for 2020[26] and adjusted to 2024 based on relative changes in total marketed oil and gas production[23] (Supplementary Note 3). Hatched light blue bars indicate regions where MethaneSAT estimates exceed inventory values, while dark blue bars indicate the opposite. Black diamond markers represent the absolute difference between MethaneSAT and inventory estimates. Bubble plots display total oil and gas production in petajoules per year (black symbols) and gas flaring volumes in billion cubic meters based on VIIRS[25] estimates (light yellow symbols) for 2024. Supplementary Fig. 6 shows the comparison for all 34 regions.

At the opposite end of the spectrum, the lowest-emitting regions (less than 20 tonnes per hour) correspond to areas with comparatively low volumes of marketed oil and gas production and minimal gas flaring activity (see Supplementary Fig. 6 for all regions). Examples include the Uinta and Greater Green River Basin in the U.S., the Tarim region in China, and the Bowen–Surat region in Australia. These low emission levels likely reflect, among other factors, the basin maturity, the prevalence of low-production wells with limited gas gathering and processing infrastructure, and the absence of significant new oil and gas exploration or development. As noted in previous studies,[14,27] small fugitive and vented methane sources from aging, low-producing infrastructure can cumulatively contribute to substantial regional emissions, representing an additional area for targeted methane mitigation. The pronounced heterogeneity revealed by these observations underscores the importance of region-specific assessments of total oil and gas methane emissions to accurately identify and prioritize mitigation opportunities.

In specific regions, empirical methane emissions exceed emission-factor-based inventories by substantial margins. Consistent with a broad body of recent peer-reviewed research[10-12,19-21], we find that, in aggregate, MethaneSAT-derived oil and gas methane emissions are approximately 60% higher than those reported to the United Nations Framework Convention on Climate Change (UNFCCC) based on the Global Fuel Exploitation Inventory (GFEI v3)[26], which serves as reference “bottom-up” country-reported inventories for all regions. At the global scale, this difference—about 10 Tg per year—is not statistically significant at the 5% level (*t*-statistic = 0.01, $p = 0.99$). Figure 3b also shows that the MethaneSAT-derived oil and gas methane emissions are 25% higher than the CAMS[24] (Copernicus Atmosphere Monitoring Service) inventories, which uses the EDGAR[28] inventory as baseline “bottom-up” estimates and adjusts estimated emissions using atmospheric inversions. We find similar discrepancies between MethaneSAT-derived estimates and inventories for the US-only regions (Fig. 3b). However, as shown below, substantial discrepancies emerge at the regional level concomitant with variability in regional oil and gas production characteristics and associated natural gas (co-produced in predominantly oil production regions) management practices.

Although inventories underestimate emissions overall, regional analysis reveals uneven performance. The UNFCCC inventory exhibits both significant underestimations and overestimations, with absolute differences ranging from less than 5 t h^{-1} to more than 200 t h^{-1} (Figs. 2 and 3b). Overestimations occur primarily in oil-dominated regions with extensive associated gas flaring, such as in Iran, Iraq, and the United Arab Emirates (Fig. 2). In contrast, underestimations are most pronounced in gas-dominated or mixed-

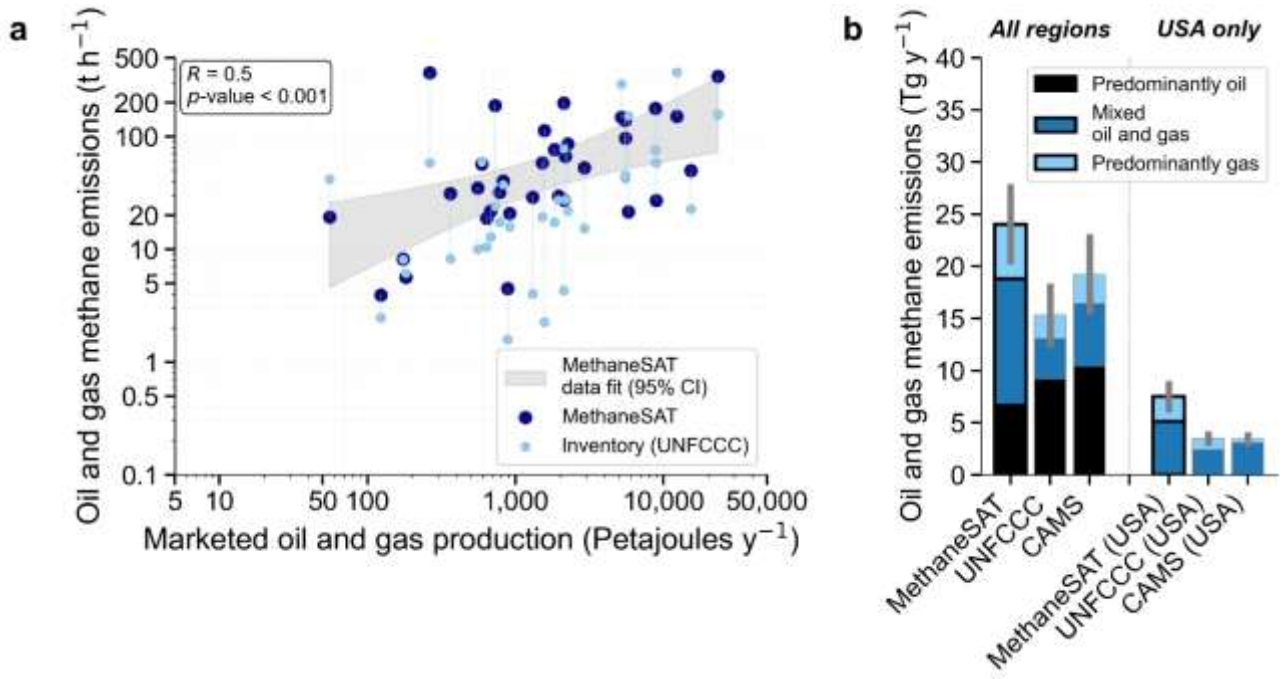


Figure 3. a. Relationship between oil and gas methane emissions and marketed oil and gas production. MethaneSAT estimates are shown as dark blue symbols, and inventory estimates (UNFCCC, GFEI) as light blue symbols. The shaded gray area represents the 95% confidence interval for an ordinary least squares (OLS) regression of MethaneSAT-derived emissions as a function of marketed oil and gas production (R = 0.5, p < 0.001). Thin connecting lines link MethaneSAT and inventory estimates for each region, visually illustrating discrepancies between measurements and inventories. **b**. Comparison of MethaneSAT-derived oil and gas methane emissions with inventory-based estimates (UNFCCC/GFEI[26]; CAMS[24]), grouped by marketed oil and gas production characteristics, aggregated across all regions and across U.S.-only regions (n = 8). Error bars indicate the 95% confidence interval for MethaneSAT estimates and an assumed ±20% uncertainty for inventory values[29].

production regions, including, for example, the Hassi R'Mel (Algeria) and Amu Darya (Uzbekistan) regions (Figs. 1b and 2). We identify 12 regions, representing 44% of total MethaneSAT-derived emissions, where MethaneSAT estimates are at least three times greater than inventory values.

Conversely, six regions, accounting for approximately 52% of total inventory emissions, report inventory estimates that exceed MethaneSAT observations. Overall, inventories overestimate methane emissions by approximately 14% in predominantly oil-producing regions (n = 6; Fig.2a, also see Fig. 1a,b for an example), while MethaneSAT-derived emissions are 2.3× higher in predominantly gas-producing regions (n = 7; see Fig. 1e, f for an example) and 3.1× higher in mixed-oil and gas production regions (n = 16; see Fig. 1c, d for an example).

As noted in previous studies[10-14,19-21,30], these discrepancies largely stem from uncertainties and limited representativeness in the emission factors and activity data used to construct bottom-up inventories. In particular, the incomplete accounting for ephemeral, high-emission facility-scale events in major production regions is a key driver of underestimation in inventories,[11,30]. Our findings also challenge the assumption that inventories consistently underestimate emissions: in several oil-dominated regions, the UNFCCC inventories overestimate methane emissions, suggesting methodological limitations and potential biases that inflate methane estimates in these contexts, especially when relying on the default IPCC Tier 1 emission factors for oil systems, which are generally higher than those for gas systems.[31]

Persistent gaps between measurement-based and inventory-based estimates across major oil and gas production regions underscore the urgent need to improve bottom-up inventories. In the absence of comprehensive, measurement-based estimates, “bottom-up” inventories play an important role as baseline estimates for assessing mitigation performance and guiding policy. As such, enhancing inventory accuracy is essential for effective methane management, as has been explored in recent research[32,33].

Methane intensity metrics provide a clear indication of the scale of avoidable methane emissions across different regions. We evaluate regional methane intensities using two complementary metrics: (i) the percentage of methane lost relative to marketed methane production (gas-normalized methane intensity) and (ii) the methane emitted per unit of marketed energy (kg per GJ; energy-normalized methane intensity). The latter metric reflects the climate intensity of oil and gas energy supply, whereas the former characterizes the effectiveness of methane control measures[34].

Across all regions, we estimate an average methane intensity of 2.9% of marketed gas production (95% confidence interval: 2.4% to 3.3%) and 0.19 kg GJ^{-1} (0.16—0.22 kg GJ^{-1}). In the U.S.-only regions (Fig. 1), we estimate methane intensities of 1.5% (1.3% to 1.8%) of marketed gas production and 0.17 kg GJ^{-1} (0.14 to 0.19 kg GJ^{-1}) relative to total oil and gas production. We note that the U.S.-only intensity metrics are for the eight regions included in this study that represent approximately 70% of U.S. onshore oil and gas production.

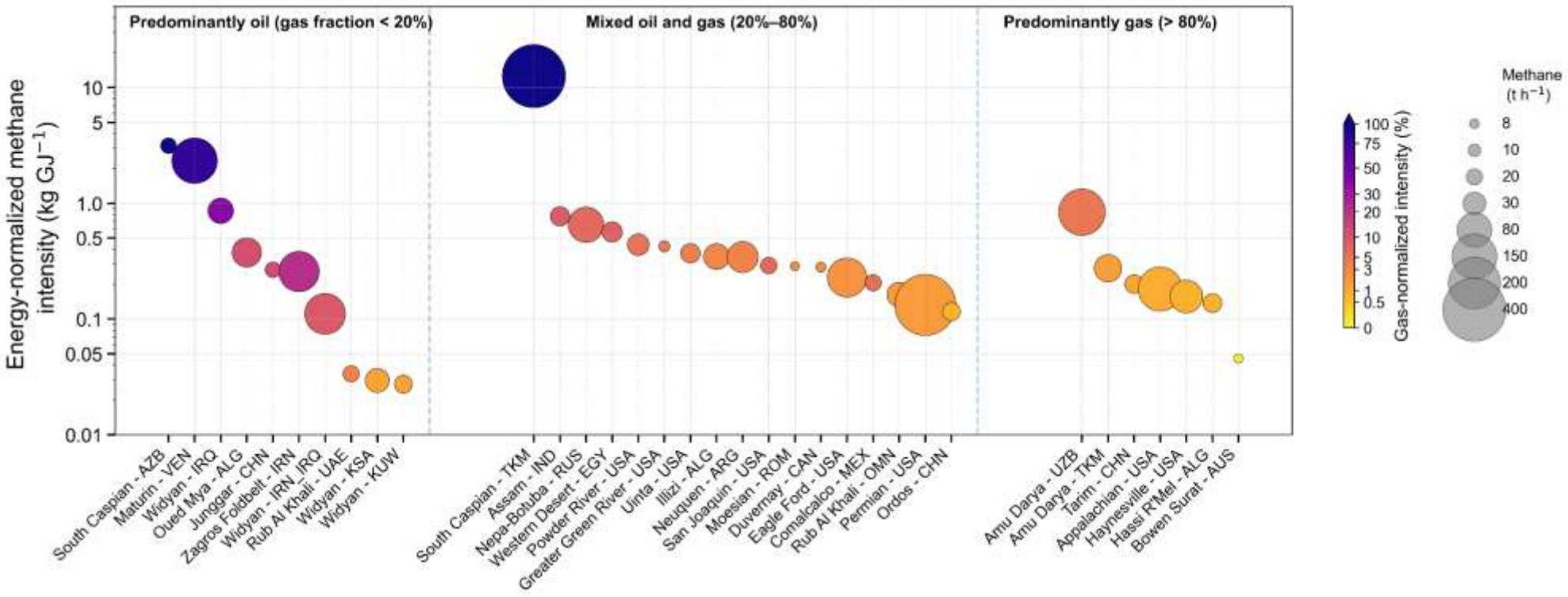


Figure 4. Comparison of oil and gas energy-normalized methane intensities by region and by oil and gas production characteristics (i.e., predominantly oil-producing, mixed oil and gas, and predominantly gas producing). The left y-axis and the bubbles show the energy-normalized methane intensity per region. The bubbles are color-coded by gas-production-normalized energy intensity (percent of marketed gas production emitted as methane) and sized by the amount of oil and gas emissions in tonnes per hour.

As shown in Fig. 4, regional energy-normalized methane intensities span more than two orders of magnitude, from less than 0.03 kg GJ^{-1} to more than 10 kg GJ^{-1}. Similarly, gas-production-normalized methane intensities show wide variation, from 0.25% to greater than 50% (Fig. 4). Importantly, this wide variation is present within each production cohort (predominantly oil, predominantly gas, and mixed), indicating that energy-normalized methane intensities are not dependent on oil and gas production profiles (Supplementary Fig. 6).

The regions with the lowest energy-normalized methane intensities are large, predominantly oil-producing basins such as Widyan in Saudi Arabia and Kuwait, which exhibit values of approximately 0.03 kg GJ^{-1} (gas-production-normalized methane intensities of ~1% to 2%, Fig. 4). These oil production regions are in countries that are signatories to the Global Methane Pledge and whose national oil companies have adopted strategic initiatives to monitor and manage methane emissions. Such measures include reducing routine flaring through expanded gas-capture infrastructure, enhancing leak detection and repair (LDAR) programs, modernizing facilities to reduce methane slip, and utilizing satellite remote sensing to support targeted abatement[35,36]. For example, Saudi Aramco has pursued decades-long efforts to eliminate routine gas flaring through its Master Gas System and associated flare-gas recovery technologies[33] and has implemented a comprehensive LDAR program complemented by regular satellite surveillance of large emitters[36].

At the opposite extreme, we identify the South Caspian region of Turkmenistan and the Maturín region of Venezuela as among the most methane-intensive regions in our analysis, each exceeding 3 kg GJ^{-1}. In both cases, methane emissions surpass reported marketed methane (gas) production (marketed gas-normalized methane intensities greater than 100%; Fig. 4), indicating pervasive leakage and venting. In Venezuela, aging oil and gas infrastructure and insufficient gas-gathering and capture systems contribute to extensive methane losses through leaks, venting, and flaring. These challenges are compounded by limited institutional capacity, weakened monitoring, reporting, and verification (MRV) systems, and the absence of robust, transparent national methane-mitigation regulations tailored to the oil and gas sector.[37] Venezuela has also not joined methane-specific international commitments such as the Global Methane Pledge[9].

Similar methane management challenges contribute to elevated intensities in Turkmenistan's South Caspian region, where outdated infrastructure, routine venting, and recurrent large-scale leaks are well documented. Numerous studies have identified methane "super-emitters" within Turkmenistan's oil and gas systems.[17,18, 38-40] Unlike Venezuela, however, Turkmenistan has publicly committed to improving methane

management. Turkmengas, the state-owned energy company, has announced initiatives to enhance gas capture, expand satellite-based monitoring, and strengthen operational controls at major gas fields[41]. Turkmenistan has also joined the Global Methane Pledge, committing to reduce methane emissions by at least 30% by 2030, though national methane-specific regulatory frameworks in the oil and gas sector remain only partially developed[41].

Our analysis also shows that the Permian Basin—one of the world's most prolific oil and gas production regions—recorded a methane intensity of approximately 0.13 kg GJ^{-1}, or approximately two percent of marketed gas production in 2024. This places the Permian below, but still broadly comparable to, several global regions with energy-normalized intensities between 0.1 and 0.5 kg GJ^{-1} (Fig. 4). The heightened scrutiny of Permian methane emissions in recent years[17,18,42,43] has likely contributed to the measurable reductions in methane intensity, even with continued growth in oil and gas production. Progress has likely been driven in part by federal and state-specific methane policies, including the U.S. EPA's Methane Emissions Reduction Program,[44] the revised New Source Performance Standards[45], and the federal methane fee on major emitters (U.S. Waste Emissions Charge[46]). Together, these policies combine mandatory equipment- and operations-based standards with incentives designed to accelerate mitigation, although recent legislative actions may influence the scope and implementation of certain program elements[47]. At the state level, New Mexico has enacted more stringent methane-control regulations, including the Methane Waste Rule[48], which is hypothesized to have contributed to recent reductions in gas-normalized methane intensities in the New Mexico portion of the Permian[17,43].

Policy implications for global oil and gas methane mitigation. Across all regions evaluated herein, we estimate that total oil and gas methane emissions correspond to approximately $350,000 USD per hour in lost revenue, assuming the average annual Henry Hub natural gas price in 2024 (~$2.1 per MMBtu).[49] This estimate underscores the substantial aggregate economic losses associated with methane leakage from oil and gas operations across these regions and highlights the need to strengthen and expand targeted methane mitigation efforts.

To compare methane mitigation performance across all regions, we benchmark each region's energy-normalized methane intensity against a target of 0.03 kg per gigajoule, equivalent to the Oil and Gas Decarbonization Charter (OGDC)[8] gas-production-normalized methane intensity target of 0.2 percent. We also compare measured methane intensities against an energy-normalized methane intensity threshold of 0.017 kg per gigajoule, which assumes an oil-only system in which associated gas produced is flared at 98% efficiency (see Supplementary Note 2 for detailed discussion). These

thresholds reflect methane performance consistent with leading industry commitments toward oil and gas methane reductions. Our analysis indicates that all assessed regions, except two regions (Widyan regions in Saudi Arabia and Kuwait) exceed the 0.03 kg GJ^{-1} target, while all regions exceed the 0.017 kg GJ^{-1} oil-only threshold. In most cases, methane intensities are more than fivefold higher than the target (Fig. 5), and in the most methane-intensive regions are >50 times greater than the intensity threshold. These findings underscore substantial shortcomings in methane management practices and highlight the scale of effort required to align with industry commitments under the OGDC and Global Methane Pledge.

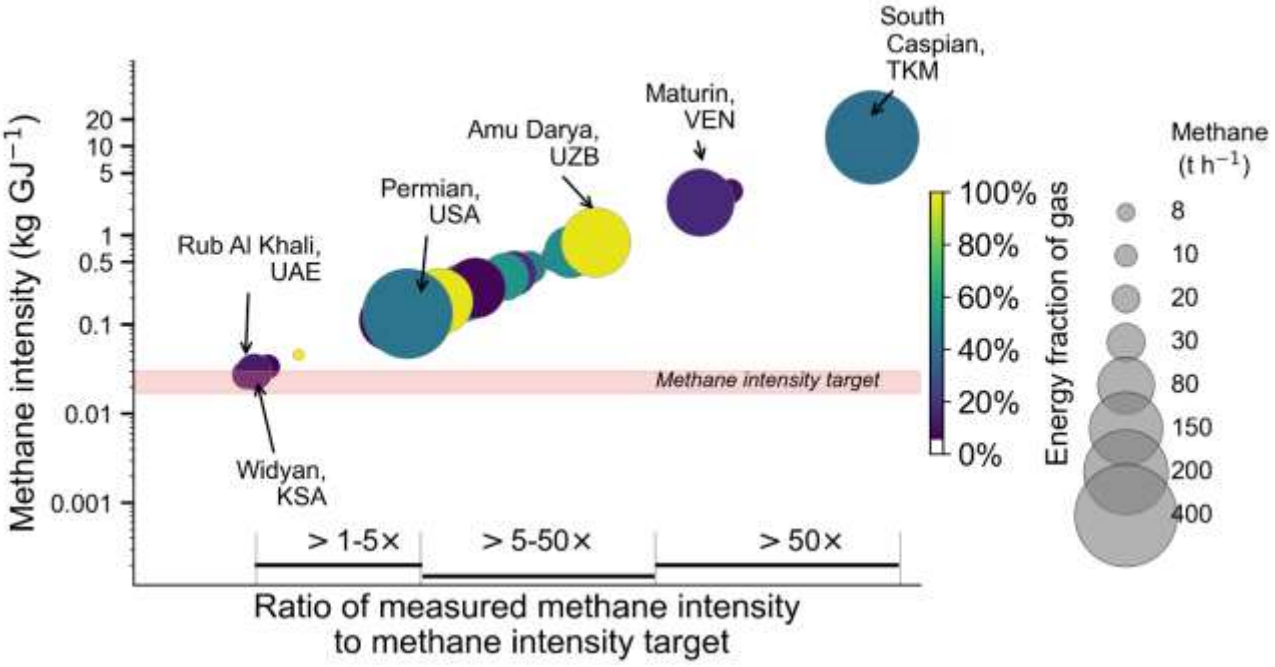


Figure 5. Comparing energy-normalized methane intensities (in kg GJ^{-1}) relative to methane intensity target of 0.017 kg GJ^{-1} (oil-only system) and 0.03 kg GJ^{-1} (equivalent to the OGDC target of 0.2 percent of marketed natural gas production), shown by the shaded red region. The x-axis shows the ratio of measured intensity to the OGDC methane intensity for each region (0.03 kg GJ^{-1}). Individual regions are shown as bubble plots, color-coded by the energy fraction of gas (% of total energy production coming from gas) and sized by the estimated oil and gas methane emissions in t h^{-1}. KSA—Kingdom of Saudi Arabia; TKM—Turkmenistan; UAE—United Arab Emirates; USA—United States of America; UZB—Uzbekistan; VEN—Venezuela.

Based on this study's results, we suggest that effective methane mitigation will require coordinated, system-wide reforms that strengthen measurements, accelerate abatement, and align regulatory and market frameworks. Priority actions include expanding robust measurements (including those that produce comprehensive total methane emissions assessments incorporating both small emitters and large "super" emitters), reporting, and verification systems; deploying high-frequency leak detection

and rapid super-emitter response (such as is currently undertaken through the UNEP MARS[50] program); eliminating routine flaring and venting through improved gas capture and utilization; and modernizing equipment across aging oil and gas production, gathering, and processing infrastructure. Moreover, as noted by Omara et al.,[14] in regions characterized by substantial numbers of marginally producing, end-of-life wells, comprehensive methane abatement policies must evaluate the economic feasibility of their continued operation under stringent emissions controls and, where such operation is not viable, identify mechanisms to finance appropriate plugging and abandonment. Given that many producing regions around the world exceed the 0.03 kg per gigajoule methane-intensity benchmark by one to two orders of magnitude, incremental improvements will not suffice. Achieving the 2030 methane-reduction goals will require a combination of rapid adoption of best-available methane abatement technologies, comprehensive MRV (monitoring, reporting and verification) integration, and enforceable mitigation standards.

Methods

Study regions

MethaneSAT was designed to quantify methane emission fluxes (kilograms per hour per square kilometer) across global regions representing at least 80% of onshore oil and gas production. A secondary objective was to characterize methane fluxes in regions where methane emissions are primarily driven by agricultural activities. The unexpected loss of satellite contact in June 2025 constrained the extent to which these objectives could be met.

The satellite instrument provided wide-area mapping capabilities, with an approximate 220 km × 220 km swath at nadir, a native spatial resolution of 110 m × 400 m, and high measurement precision (2.5–5.5 ppb at 2 km × 2 km aggregation).[22] These specifications enabled the retrieval of basin-scale xCH_4 concentration data suitable for quantifying both diffuse area-source emissions and discrete high-emitting point sources.

The selection of MethaneSAT targets focused on major global oil and gas production regions. Each target covered approximately 200 km × 200 km and was centered on the major oil and gas production fields and dense infrastructure zones. Additional indicators of oil and gas emission activity, including gas flaring and previously identified methane hotspots, were used to refine target placement and optimize coverage. Practical satellite observability constraints—e.g., cloud cover, wind speed and direction, solar zenith angle, surface reflectivity, and terrain complexity—also informed both the feasible target location and achievable sampling frequency.

All oil and gas targets included in this study were observed at least once between May 2024 and June 2025. The final spatial extent of each mapped area, or of aggregated neighboring targets (hereafter referred to as “regions”), was determined by the boundaries of the MethaneSAT inversion domains —which could exclude cloudy areas (as described below)—and by the spatial consolidation of adjacent and overlapping observations. Each aggregated domain had MethaneSAT observations ranging from one to 20 observations between May 2024 and June 2025. Figure 1 shows the locations of the 34 regions included in this study, which together accounts for approximately one-half of global onshore oil and gas production. Additional details for each region, including the number of observations, total methane emissions, total oil and gas methane emissions and methane intensities can be found in Supplemental Data 1. Supplemental Data 2 includes geospatial data (.geojson) of the study domains for each region.

MethaneSAT L4 inversion methodology

The MethaneSAT L4 Column Observations to Regional Emissions (CORE) algorithm is designed to estimate spatially distributed total methane emissions by solving an inverse model that ingests MethaneSAT XCH_4 observations (L3), meteorology from the Global Forecast System (NOAA, 2015-present), a model of topographic variation in background XCH_4, and a weakly informative lognormal prior (ensuring positivity) as inputs. Full details of the CORE inversion methodology can be found in the CORE ATBD.[51] Briefly, we use the Stochastic Time-Inverted Lagrangian Transport (STILT)[52] model to compute the Jacobian that links upwind fluxes to observed enhancements, and emissions and background terms are jointly inferred using the Stan[53] No-U-Turn Sampler (NUTS[54]). Equation 1 describes the inversion framework:

$$z = J_{int}s_{int} + J_{ext}s_{ext} + (z_{prior} + Ab)$$

where z is the vector of observed xCH_4 values, J is the Jacobian matrix describing the sensitivity of each observation to surface emissions, s represents methane emission rates within the interior and exterior domains, z_{prior} is the prior methane column used in the Level-2 retrieval, A is the averaging kernel, and b is a background offset parameter.

The source–receptor relationship represented by J is computed using STILT driven by meteorological fields from the Global Forecast System. STILT simulates backward particle trajectories from observation locations to quantify the sensitivity of each observation to upwind methane emissions. The inversion estimates posterior emission distributions by sampling parameter values that jointly maximize consistency with the observations and prior constraints under the Bayesian model. To capture upwind

variability efficiently, exterior emitters are clustered into 350 groups using K-means[55] on cosine distances of their STILT footprints, reducing parameter collinearity while preserving expressivity of the boundary-inflow model. STILT footprints extend 28 hours upwind (a typical ventilation timescale for scene size and winds), such that each emissions map represents up to 28-hour effective averaging window, which partially smooths diurnal variability[56].

MethaneSAT Level-3 observations are aggregated to 2 km × 2 km grids prior to inversion to reduce measurement noise and computational cost. The total methane emissions are estimated on a 4 km × 4 km grid within an interior domain defined by contiguous regions of valid observations, while potential methane emission sources extending up to 300 km beyond the observed domain are included to represent inflow contributions through atmospheric transport. The background methane column is represented as the retrieval prior plus an additive offset parameter scaled by the averaging kernel derived from the Level-2 methane retrieval[22]. Exterior emission sources are clustered according to the similarity of their transport footprints to reduce the dimensionality of the inverse problem.

We estimate the inversion model parameters using Bayesian inference with state vector $\theta = (s_{int}, s_{ext}, b)$ and generate posterior samples using the Stan probabilistic programming framework[53] with the No-U-Turn Sampler[54], an adaptive Hamiltonian Monte Carlo algorithm[57]. Observation uncertainty is represented by a constant standard deviation of 11 ppb, representing an aggregate instrument and unresolved transport and model error, and that errors are assumed uncorrelated at the aggregate scale. The emission rates are assigned lognormal prior distributions.

Posterior mean emission rates provide the estimated flux (total methane emissions from all methane sources) for each grid, and uncertainty in total emissions is derived from the posterior distribution (n=1,000 MCMC samples from four independent chains) through the Markov Chain Monte Carlo (MCMC) process. To reduce bias associated with small emissions that may arise due to measurement noise, we remove likely zero-emission grid cells emitting below 1 kg h^{-1} km^{-2} (noise floor) based on the Widely Applicable Information Criterion.[51] Figure 1 (panels **a, c,** and **d**) show examples of the high-resolution spatially distributed total methane emission fluxes based on MethaneSAT observations.

Aggregation of multiple MethaneSAT observations and sectoral attribution to oil and gas methane sources

We follow the procedure outlined in Williams et al.[20] to aggregate the MethaneSAT spatially explicit methane fluxes in regions with multiple observations and perform sectoral attribution to oil and gas methane sources. Briefly, we reproject all emission maps onto a common 0.04° × 0.04° global grid using an equal-area weighting scheme that conserves total methane mass. Emission rates from overlapping scenes are then averaged to generate an aggregated emission map and spatial extent. We assess uncertainties in the aggregated MethaneSAT emissions estimates leveraging the 4,000 samples drawn from each grid's MCMC posterior distribution, representing the mean-level uncertainty for that location. When multiple emissions maps contribute to a single grid, 4,000 combined cell-level estimates are produced by repeatedly drawing one value from each map with replacement and averaging the results. This Monte Carlo resampling propagates uncertainty through the arithmetic mean without requiring assumptions about the shape of the resulting distribution. The procedure is applied independently to all subregions defined by unique combinations of overlapping emissions maps. For each of the 4,000 iterations, summing across all subregions yields one estimate of total methane emissions for the aggregated domain. The 2.5th and 97.5th percentiles of the resulting distribution define the reported 95% uncertainty interval, to which an additional 20% is added to account for atmospheric transport error.

Following Williams et al.[19], we attribute MethaneSAT methane emissions to broad sectors using a proportional allocation method in which sector-level emissions are computed from the ratio of sectoral prior emissions to the total prior emissions within each region. Briefly, for any region, we develop sectoral priors by summing two bottom-up inventories selected according to region (EPA-GHGI[58], EI-ME[59], EDGAR[28] for U.S. regions; CAMS v6.2[24], GFEI v3[26], EDGAR[28] elsewhere) together with persistence-weighted satellite point source data from the Carbon Mapper Data Portal[60] (≥3 detections)), and wetland emissions from WetCHARTs (v1.3.1)[61]. We regrid the composite prior to the 0.04° × 0.04° MethaneSAT grid using equal-area mass-conserving reprojection. For regions outside the U.S., oil-and-gas emissions in the composite prior are spatially aggregated to 0.4° × 0.4° to address sparse infrastructure data.[19] We then apportion MethaneSAT total emissions across major sectors (e.g., oil and gas, landfills, coal, livestock, wetlands, and other anthropogenic sources), using the proportional relationship between composite prior sectoral contributions and prior totals. Grid cells where MethaneSAT emissions exceed composite priors by >100× are labeled "unknown" and their relative emissions to the total are incorporated into the overall sectoral uncertainties.

In addition to the primary methodology described above, we also estimate oil and gas methane emissions using a literature-based subtraction approach. Specifically, we subtract representative mean estimates of non–oil and gas methane emissions derived

from peer-reviewed studies, following the procedures outlined in MacKay et al.[62] Non–oil and gas emissions for each region are informed by data from EDGAR,[28] CAMS v6.2,[24] GFEI v3,[26] and East et al.[19] Although our primary analysis prioritizes the composite-prior methodology, which yields spatially explicit estimates of oil and gas methane emissions alongside other methane sources,[20] the literature-based subtraction approach serves two complementary purposes. First, it provides a sensitivity analysis for evaluating the robustness of our results; second, it improves estimates of oil and gas emissions in barren regions with negligible non-oil and gas sources relative to previous literature. In addition, we demonstrate that an alternative sectoral attribution approach based solely on the sectorally-resolved emissions from East et al.[19] produces oil and gas methane emission estimates that are broadly consistent with those from the primary methodology (see Supplementary Note 1 and Supplementary Fig. 1). Finally, we compare our estimate of oil and gas methane emissions based on MethaneSAT quantification with peer-reviewed estimates from global datasets provided by East et al.[19], as well as EDGAR, CAMS, and the GFEI v3 inventories. Supplementary Figs. 8—41 shows a detailed comparison of each region's aggregated total methane emissions with peer-reviewed literature ("top-down") and commonly-used "bottom-up" inventories.

Assessment of oil and gas methane intensities

Methane intensity metrics are widely used to evaluate methane emissions relative to methane production or energy output (total oil and gas production) and to assess methane management and climate performance in the oil and gas sector. In this study, we compute two complementary metrics. We estimate gas production–normalized methane intensity, defined as the percentage of methane emitted relative to marketed methane production. Marketed methane production is estimated using reported marketed natural gas volumes, assuming a methane content of 90% and a methane density of 19.2 kg per 1,000 cubic feet. We apply a uniform methane content of 90% across all regions, recognizing that the global oil and gas production data from Wood Mackenzie (www.woodmac.com) represent marketed gas volumes that exclude gas flared or reinjected and are expected to be of pipeline quality, with non-methane hydrocarbons and other impurities removed. We also assess energy-normalized methane intensity, defined as methane emitted (in kilograms) per unit of marketed energy production from oil and natural gas, expressed in gigajoules. Wood Mackenzie reports oil and gas production in units of thousand barrels of oil equivalent per day (kboed). We convert these values to gigajoules per year assuming 365 days per year and an energy content of 6.1 gigajoules per barrel of oil equivalent. Marketed oil and gas production data for 2024, obtained from Wood Mackenzie, are used to normalize regional methane emissions and derive the reported intensity values.

The oil and gas production data from Wood Mackenzie, while spatially explicit and temporally resolved on an annual basis, are available only at the “asset” level (typically corresponding to individual oil and gas fields, each of which may include tens to thousands of production wells and associated gathering and processing infrastructure). In most cases, asset boundaries fall entirely within aggregated MethaneSAT regions. Where asset geometries partially overlap a MethaneSAT region, we apply an area-weighted approach to adjust field-level production estimates based on the fraction of the asset area intersecting the region of interest. Supplementary Note 2 includes additional discussion on methane intensity metrics and oil and gas production ratios

Method and Data Uncertainties

The uncertainty in the CORE inversion results are estimated from two components: first, the posterior uncertainty is derived from the Bayesian inversion and includes uncertainties arising from measurement noise and the partitioning between the interior emissions and the boundary inflow. These uncertainties are summarized using the 95th percentile range of the bootstrap resampling of the 4,000 MCMC samples. Second, an additional 20% empirical uncertainty is applied to account for meteorological transport errors introduced during the Jacobian generation. These errors are not explicitly represented in the inverse model.

To estimate uncertainties associated with the sectoral attribution of total methane emissions, we apply bootstrap resampling (n = 4,000) to the inputs used to construct the prior emissions estimates in the stacked prior inventory. These resampled priors are then used to recompute the sectoral disaggregation. For the bottom-up inventories, regardless of sector, we assume grid-level emissions follow a normal distribution with a standard deviation of 50%. For the satellite-based point source data[60], we use the provided source-level standard deviations and assume normally distributed emission rates for resampling (n = 4,000). Sectoral emission ratios are calculated 4,000 times using these resampled inputs to derive upper and lower bounds for sector-specific methane emissions. The 2.5th and 97.5th percentiles of these ratios define the uncertainty in sectoral disaggregation, including contributions from unknown methane emissions. The additional uncertainty associated with attributing MethaneSAT-detected unknown emissions contribute less than 1% to total uncertainty for all regions analyzed in this study.

Our comparison of MethaneSAT oil and gas methane emissions with reported bottom-up inventories is subject to uncertainties arising from differences in the reporting periods of the underlying datasets. MethaneSAT emission estimates are derived from short-duration satellite observations and inversions that represent emissions over a temporal window of up to 28 hours preceding the observation. In contrast, bottom-up

inventories typically report average annual methane emissions. While we compare inventory data for the same year as MethaneSAT observations, we acknowledge the difficult-to-quantify uncertainties associated with temporal variability between MethaneSAT observations and inventory estimates used herein. Finally, we acknowledge uncertainties related to the reported marketed oil and gas production data, which are available internationally on an annual basis and may be subject to reporting errors that are difficult to quantify.

References

1. Etminan, M., Myhre, G., Highwood, E. J. & Shine, K. P. Radiative forcing of carbon dioxide, methane, and nitrous oxide: a significant revision of the methane radiative forcing. *Geophys. Res. Lett.* **43**, 12,614–12,623 (2016) https://doi.org/10.1002/2016GL071930
2. Intergovernmental Panel on Climate Change. *Climate Change 2021: The Physical Science Basis*. Contribution of Working Group I to the Sixth Assessment Report of the Intergovernmental Panel on Climate Change (Cambridge Univ. Press, 2021). https://www.ipcc.ch/report/ar6/wg1/
3. Saunois, M. *et al.* The global methane budget 2000–2017. *Earth Syst. Sci. Data* **12**, 1561–1623 (2020). https://doi.org/10.5194/essd-12-1561-2020
4. Ocko, I.B. *et al.* Acting rapidly to deploy readily available methane mitigation measures by sector can immediately slow global warming, *Environ. Res. Lett.* **16** 054042 (2021) https://doi.org/10.1088/1748-9326/abf9c8
5. Kemp, C.E., Ravikumar, A.P. New technologies can cost effectively reduce oil and gas methane emissions, but policies will require careful design to establish mitigation equivalence. *Environ. Sci. Technol.* **55,** 13, 9140-9149 (2021) https://doi.org/10.1021/acs.est.1c03071
6. Tyner, D.R., Johnson, M.R. A techno-economic analysis of methane mitigation potential from reported venting at oil production sites in Alberta. *Environ. Sci. Technol.* 2018, **52**, 21, 12877–12885 (2018) https://doi.org/10.1021/acs.est.8b01345
7. UNFCCC. The United Nations Framework Convention on Climate Change. The Paris Agreement (2015). https://unfccc.int/process-and-meetings/the-paris-agreement
8. OGDC. The Oil and Gas Decarbonization Charter. Available online at https://www.ogdc.org/oil-gas-decarbonization-charter/ Last accessed March 11, 2026.
9. The Global Methane Pledge. https://www.globalmethanepledge.org/ Last accessed March 11, 2026
10. Zavala-Araiza, D. *et al.* Reconciling divergent estimates of oil and gas methane emissions. *Proc. Natl Acad. Sci. USA* **112**, 15597–15602 (2015). https://doi.org/10.1073/pnas.1522126112
11. Brandt, A. R., Heath, G. A. & Cooley, D. Methane leaks from natural gas systems follow extreme distributions. *Environ. Sci. Technol.* **50**, 12512–12520 (2016). https://doi.org/10.1021/acs.est.6b04303

12. Alvarez, R. A. *et al.* Assessment of methane emissions from the U.S. oil and gas supply chain. *Science* **361**, 186–188 (2018). https://doi.org/10.1126/science.aar7204
13. Worthy, D. E. J. *et al.* Hybrid bottom-up and top-down framework resolves discrepancies in Canada's oil and gas methane inventories. *Commun. Earth Environ.* **5**, 566 (2024). https://doi.org/10.1038/s43247-024-01728-6
14. Omara, M., Zavala-Araiza, D., Lyon, D.R. *et al.* Methane emissions from US low production oil and natural gas well sites. *Nat Commun* **13**, 2085 (2022). https://doi.org/10.1038/s41467-022-29709-3
15. Lauvaux, T. *et al.* Global assessment of oil and gas methane ultra-emitters. *Science* 375, **6580**, 557-561 (2022) https://doi.org/10.1126/science.abj4
16. Schuit, B.J. et al. Automated detection and monitoring of methane super-emitters using satellite data. *Atmos. Chem. Phys.,* **23**, 9071–9098 (2023) https://doi.org/10.5194/acp-23-9071-2023
17. Varon, D.J. *et al.* Continuous weekly monitoring of methane emissions from the Permian Basin by inversion of TROPOMI satellite observations. *Atmos. Chem. Phys.,* **23**, 7503–7520 (2023) https://doi.org/10.5194/acp-23-7503-2023
18. Guanter, L. *et al.* Surveying Methane Point-Source Super-Emissions across Oil and Gas Basins with MethaneSAT. *Atmos. Chem. Phys.,* **26**, 2941–2963 (2026), https://doi.org/10.5194/acp-26-2941-2026, 2026.
19. East, J.D., Jacob, D.J., Jervis, D. *et al.* Worldwide inference of national methane emissions by inversion of satellite observations with UNFCCC prior estimates. *Nat Commun* **16**, 11004 (2025). https://doi.org/10.1038/s41467-025-67122-8
20. Williams, J.P. *et al.* Methane intensity and emissions across major oil and gas basins and individual jurisdictions using MethaneSAT observations. Atmos. Chem. Phys., 26, 5961–5981, https://doi.org/10.5194/acp-26-5961-2026, 2026.
21. Shen, L., Jacob, D.J., Gautam, R. *et al.* National quantifications of methane emissions from fuel exploitation using high resolution inversions of satellite observations. *Nat Commun* **14**, 4948 (2023). https://doi.org/10.1038/s41467-023-40671-6
22. Chan Miller, C. *et al.* Methane retrieval from MethaneAIR using the CO_2 proxy approach: a demonstration for the upcoming MethaneSAT mission. *Atmos. Meas. Tech.,* 17, 5429–5454 (2024), https://doi.org/10.5194/amt-17-5429-2024
23. Wood Mackenzie. Asset-level oil and gas production data. www.woodmac.com (2026). Last accessed March 11, 2026
24. van der Gon, H.D. et al. Documentation of the CAMS emission inventory products. Available online at https://atmosphere.copernicus.eu/node/1054 , https://doi.org/ 10.24380/q2si-ti6i (2023)
25. Elvidge, C.D. *et al.* VIIRS nightfire: Satellite pyrometry at night. *Remote Sens.* 5, 9, 4423-4449, https://doi.org/10.3390/rs5094423 (2013)
26. Scarpelli, T. R. *et al.* Using new geospatial data and 2020 fossil fuel methane emissions for the Global Fuel Exploitation Inventory (GFEI) v3. Earth Syst. Sci. Data, 17, 7019–7033, https://doi.org/10.5194/essd-17-7019-2025, 2025.
27. Williams, J. P. *et al.* Small emission sources in aggregate disproportionately account for a large majority of total methane emissions from the US oil and gas

sector, *Atmos. Chem. Phys.,* 25, 1513–1532 (2025), https://doi.org/10.5194/acp-25-1513-2025
28. Crippa, M. *et al.* Insights into the spatial distribution of global, national, and subnational greenhouse gas emissions in the Emissions Database for Global Atmospheric Research (EDGAR v8.0), Earth System Science Data, 16, 2811–2830 (2024), https://doi.org/10.5194/essd-16-2811-2024
29. U.S. Environmental Protection Agency. Inventory of U.S. Greenhouse Gas Emissions and Sinks: 1990-2022. Available online at https://www.epa.gov/ghgemissions/inventory-us-greenhouse-gas-emissions-and-sinks-1990-2022. Last accessed March 11, 2026
30. Zavala-Araiza, D., Alvarez, R., Lyon, D. *et al.* Super-emitters in natural gas infrastructure are caused by abnormal process conditions. *Nat Commun* **8**, 14012 (2017). https://doi.org/10.1038/ncomms14012
31. Intergovernmental Panel on Climate Change. Guidelines for national greenhouse gas inventories (2006). Available online at https://www.ipcc-nggip.iges.or.jp/public/2006gl/pdf/2_Volume2/V2_4_Ch4_Fugitive_Emissions.pdf. Last accessed March 11, 2026.
32. Hancock, S.E. *et al.* Applying Satellite Observations to Improve Bottom-Up National Emission Inventories for Methane: Application to Colombia; EGUsphere [preprint], https://doi.org/10.5194/egusphere-2025-5478, 2026
33. Zhu, Q. et al. Advancements and opportunities to improve bottom–up estimates of global wetland methane emissions. *Environ. Res. Lett.* **20** 023001 (2025), https://doi.org/10.1088/1748-9326/adad02
34. Seymour, S.P. et al. Methane intensity metrics: unmasking the trade-offs. [Preprint] https://doi.org/10.21203/rs.3.rs-6753363/v1 (2025)
35. Saudi Aramco: Methane Mitigation Efforts. Available online at https://globalmethane.org/challenge/saudiaramco.html. Last accessed March 11, 2026
36. Kingdom of Saudi Arabia. Methane Emissions Mitigation in the Oil and Gas Industry in Saudi Arabia. https://www.globalmethane.org/documents/2024Forum/Oil%20&%20Gas%20Sessions/1%20-%20Governments%20as%20Vital%20Drivers%20to%20Mobilize%20Methane%20Action%20in%20the%20Oil%20&%20Gas%20Sector/1%20-%20Al%20Qurooni_Methane%20Emissions%20Mitigation%20in%20Saudi%20Arabia_Oil%20&%20Gas.pdf Last accessed March 11, 2026
37. U.S. Energy Information Administration. Country Analysis Brief: Venezuela. Available online at https://www.eia.gov/international/analysis/country/VEN , last accessed March 11, 2026.
38. He, Z. et al. Satellite insights into methane super-emitters: regional emissions and yearly growth on Turkmenistan's west coast. *Int. J. Appl. Earth Observ. Geo.* 145, 104975 (2025) https://doi.org/10.1016/j.jag.2025.104975
39. Varon, D.J. et al. Satellite discovery of anomalously large methane point sources from oil/gas production. *Geophys. Res. Lett.* **46**, 22, 13507-13516 (2019). https://doi.org/10.1029/2019GL083798

40. Jervis, D. Global energy sector methane emissions estimated by using facility-level satellite observations. *Science.* **390**, 6778, 1151-1155 (2025) https://doi.org/10.1126/science.adv3
41. Government of Turkmenistan. Turkmenistan's achievements in reducing methane emissions were announced at the TESC 2025 Conference. Available online at https://www.oilgas.gov.tm/en/posts/news/14198/turkmenistans-achievements-in-reducing-methane-emissions-were-announced-at-the-tesc-2025-conference. Last accessed March 11, 2026
42. Zhang, Y. et al. Quantifying methane emissions from the largest oil-producing basin in the United States from space. *Sci. Adv.* 6, 17 (2020), https://doi.org/10.1126/sciadv.aaz5120
43. Varon. D.J. et al. Seasonality and declining intensity of methane emissions from the Permian and nearly US oil and gas basins. *Env. Sci. Technol.* 60, 1, 425-435 (2026) https://doi.org/10.1021/acs.est.5c08745
44. U.S. Environmental Protection Agency. Methane Emissions Reduction Program. Available online at https://www.epa.gov/inflation-reduction-act/methane-emissions-reduction-program. Last accessed March 11, 2026
45. U.S. Environmental Protection Agency. EPA's Final Rule to Reduce Methane and Other Harmful Pollution from Oil and Natural Gas Operations and Related Actions. Available online at https://www.epa.gov/controlling-air-pollution-oil-and-natural-gas-operations/epas-final-rule-reduce-methane-and-other. Last accessed March 11, 2026.
46. U.S. Federal Register. Waste emissions charge for petroleum and natural gas systems: procedures for facilitating compliance, including netting and exemptions. Available online at https://www.federalregister.gov/documents/2024/11/18/2024-26643/waste-emissions-charge-for-petroleum-and-natural-gas-systems-procedures-for-facilitating-compliance. Last accessed March 11, 2026
47. U.S. Congress. H.J.Res.35 - Providing for congressional disapproval under chapter 8 of title 5, United States Code, of the rule submitted by the Environmental Protection Agency relating to "Waste Emissions Charge for Petroleum and Natural Gas Systems: Procedures for Facilitating Compliance, Including Netting and Exemptions". Available online at https://www.congress.gov/bill/119th-congress/house-joint-resolution/35/text?s=1&r=4 Last accessed March 11, 2026
48. New Mexico Energy, Minerals, and Natural Resources Department. Methane Waste Rule. Available online at https://www.emnrd.nm.gov/ocd/methane-waste-rule/. Last accessed March 11, 2026
49. Henry Hub Natural Gas Spot Price. https://www.eia.gov/dnav/ng/hist/rngwhhdA.htm, last accessed on March 11, 2026.
50. United Nations Environment Program. Methane Alert and Response System. Available online at https://www.unep.org/topics/energy/methane/how-mars-works. Last accessed March 11, 2026.

51. The MethaneSAT Science and Engineering Team: MethaneSAT Level-4 Dispersed Emissions Product: Algorithm Theoretical Basis Document v1.1, https://doi.org/10.5281/zenodo.19873046, 2026.
52. Fasoli, B. *et al.* Simulating atmospheric tracer concentrations for spatially distributed receptors: updates to the Stochastic Time-Inverted Lagrangian Transport model's R interface (STILT-R version 2), *Geosci. Mod. Dev.,* 11, 2813–2824 (2018), https://doi.org/10.5194/gmd-11-2813-2018.
53. Carpenter, B. *et al.* Stan: A Probabilistic Programming Language, Journal of Statistical Software, 76, 1–32 (2017), https://doi.org/10.18637/jss.v076.i01, 2017.
54. Hoffman, M. D. and Gelman, A.: The No-U-Turn Sampler: Adaptively Setting Path Lengths in Hamiltonian Monte Carlo, https://doi.org/10.48550/arXiv.1111.4246, 18 November 2011.
55. Ester, M., Kriegel, H.-P., Sander, J., and Xu, X.: A density-based algorithm for discovering clusters in large spatial databases with noise, in: kdd, 226–231 (1996).
56. Vechi, N. T., Mellqvist, J., Samuelsson, J., Offerle, B., and Scheutz, C.: Ammonia and methane emissions from dairy concentrated animal feeding operations in California, using mobile optical remote sensing, Atmos. Env. 293, 119448 (2023), https://doi.org/10.1016/j.atmosenv.2022.119448.
57. Neal, Radford. 2011. "MCMC Using Hamiltonian Dynamics." In *Handbook of Markov Chain Monte Carlo*, edited by Steve Brooks, Andrew Gelman, Galin L. Jones, and Xiao-Li Meng, 116–62. Chapman; Hall/CRC.
58. Maasakkers, J. D. et al. Gridded Inventory of Annual 2012–2018 U.S. Anthropogenic Methane Emissions, Environ. Sci. Technol., 57, 16276–16288 (2023), https://doi.org/10.1021/acs.est.3c05138.
59. Omara, M. *et al.* Constructing a measurement-based spatially explicit inventory of US oil and gas methane emissions, Earth System Science Data Discussions, 1–25 (2024), https://doi.org/10.5194/essd-2024-72.
60. Carbon Mapper Data Portal. www.data.carbonmapper.org. Last accessed March 11, 2026
61. Bloom, A. A. *et al.* A global wetland methane emissions and uncertainty dataset for atmospheric chemical transport models (WetCHARTs version 1.0), Geoscientific Model Development, 10, 2141–2156 (2017), https://doi.org/10.5194/gmd-10-2141-2017.
62. MacKay, K., Benmergui, J., Williams, J. P., Omara, M., Himmelberger, A., Sargent, M., Warren, J. D., Miller, C. C., Roche, S., Zhang, Z., Franklin, J., Guanter, L., Wofsy, S., and Gautam, R.: Assessment of methane emissions from US onshore oil and gas production using MethaneAIR measurements, Atmos. Chem. Phys., 26, 1179–1192, https://doi.org/10.5194/acp-26-1179-2026, 2026.

Acknowledgments

We thank the MethaneSAT mission operations team, data processing team, and science team for the provision of data products used in this study. We acknowledge the

use of publicly available emissions datasets and analysis tools that made this work possible, including products from the Copernicus Atmosphere Monitoring Service (CAMS), the Emissions Database for Global Atmospheric Research (EDGAR), Carbon Mapper, and the Global Fuel Exploitation Inventory (GFEI v3). We further acknowledge the use of open-access satellite-based methane studies that informed and supported this analysis.

Funding for MethaneSAT activities was provided in part by anonymous donors, Arnold Ventures, The Audacious Project, the Ballmer Group, the Bezos Earth Fund, The Children's Investment Fund Foundation, the Heising–Simons Family Fund, King Philanthropies, the Robertson Foundation, the Skyline Foundation, and the Valhalla Foundation. For a more complete list of funders, please visit https://www.methanesat.org/ (last access: 5 May 2026).

Author Contributions

M.O. and R.G. contributed to the study conceptualization. M.O., J.PW., A.H., K.W., B.L., J.W., K.M., L.G., and R.G. contributed to formal data analysis and visualization. J.B., M.K., C.C.M., S.R., J.F., and S.C.W. contributed to the science algorithms development. M.O. wrote the manuscript with contributions from J.PW., A.H., K.W., B.L., J.W., K.M., L.G., J.B., M.K., C.C.M., S.R., J.F., S.C.W., S.P.H., and R.G.

Competing Interests

The authors declare no competing financial interests.

Materials and Correspondence

Mark Omara, momara@edf.org

Supplementary Information

Supplementary Information document is available and contains four Supplementary Notes and 41 Supplementary Figures. Additional data for each region are included in Supplementary Data 1. Geospatial data representing the boundary of each aggregated region is available in Supplementary Data 2.

Data availability

MethaneSAT data products are publicly accessible through Google Earth Engine:
L3 concentrations: https://developers.google.com/earth-engine/datasets/catalog/projects_edf-methanesat-ee_assets_public-preview_L3concentration (last access: 05 May 2026),
L4 emissions: https://developers.google.com/earth-engine/datasets/catalog/projects_edf-methanesat-ee_assets_public-preview_L4area_v2

(last access: 05 May 2026). The Level-1B onwards data products are additionally available via the public request links provided in either the L3 concentrations or L4 emissions data linked above.

Code availability

Python 3.12 used for data analysis and visualization are available from the authors upon reasonable request.

Supplementary Files

This is a list of supplementary files associated with this preprint. Click to download.

- OmaraetalSupplementalData1.xlsx
- OmaraetalSupplementaryData2.zip
- OmaraetalSupplementalInformation05072026.docx